# Crystal Structure of the Conserved Core of HIV-1 Nef Complexed with a Src Family SH3 Domain

Chi-Hon Lee,* Kalle Saksela,* Urooj A. Mirza,*
Brian T. Chait,* and John Kuriyan*†
*The Rockefeller University
†Howard Hughes Medical Institute
1230 York Avenue
New York, New York 10021

## Summary

The crystal structure of the conserved core of HIV-1 Nef has been determined in complex with the SH3 domain of a mutant Fyn tyrosine kinase (a single amino acid substitution, Arg-96 to isoleucine), to which Nef binds tightly. The conserved PxxP sequence motif of Nef, known to be important for optimal viral replication, is part of a polyproline type II helix that engages the SH3 domain in a manner resembling closely the interaction of isolated peptides with SH3 domains. The Nef–SH3 structure also reveals how high affinity and specificity in the SH3 interaction is achieved by the presentation of the PxxP motif within the context of the folded structure of Nef.

## Introduction

The *nef* gene of human and simian immunodeficiency viruses (HIV-1, HIV-2, and SIV) codes for a protein that is critical for the development of AIDS (reviewed by Trono, 1995). Rhesus monkeys inoculated with pathogenic strains of SIV develop an AIDS-like disease and eventually die as a consequence. Remarkably, animals infected with an isogenic strain of SIV missing Nef remain healthy and acquire long-term immunity that protects them from subsequent challenge with pathogenic strains of SIV (containing Nef) (Kestler et al., 1991; Daniel et al., 1992). Likewise, viruses defective in the *nef* gene have been isolated from some humans who are experiencing long-term nonprogressive HIV-1 infection (Kirchhoff et al., 1995; Deacon et al., 1995).

Although Nef is clearly essential for disease progression, the mechanism of its action is poorly understood. Nef enhances viral infectivity and replication in primary cells, it alters the state of T cell activation, and it reduces the surface expression of CD4, the major receptor for HIV (reviewed by Trono, 1995). Nef has no known catalytic activity and is therefore likely to function through interactions with cellular proteins, particularly those involved in cellular activation and signaling. In particular, Nef has been shown to associate with Ser/Thr protein kinase activity (Sawai et al., 1994) as well as with certain Src family tyrosine kinases (Saksela et al., 1995).

The interaction of Nef with Src family tyrosine kinases is intriguing because these proteins have diverse and critically important roles in many cellular signaling pathways (Bolen, 1993). The Src family kinases have in common a modular architecture composed of a conserved catalytic domain and two other Src homology domains, known as SH2 and SH3, that bind to phosphotyrosine-

and proline-containing sequences, respectively (reviewed by Pawson, 1995; Cohen et al., 1995a). SH3 target peptides adopt a type II left-handed polyproline helical conformation, characterized by the sequence signature PxxP, where x is any amino acid (Ren et al., 1993; Lim and Richards, 1994; Yu et al., 1994). Nef contains a highly conserved PxxP motif, and we have shown that the interaction of Nef with Src family SH3 domains is among the tightest known SH3–ligand interactions ($K_d$ = 0.25 μM for Hck SH3 and 0.38 μM for Fyn [R96I mutant] SH3) (Lee et al., 1995). The physiological relevance of the interaction of Nef with SH3 domains is unknown. However, mutagenesis of Nef showed that the PxxP motif is essential for optimal spread of HIV-1 virus in primary cell cultures, suggesting that the virus has evolved to exploit SH3-mediated interactions with cellular proteins to enhance its replication in some way (Saksela et al., 1995).

The interaction of SH3 domains with peptide ligands that contain PxxP motifs is now well understood. However, a notable feature of the Nef–SH3 interaction is that isolated peptides corresponding to the PxxP motif of Nef do not bind to the SH3 domains with high affinity (Lee et al., 1995). This suggests that other elements of the tertiary structure of a folded Nef molecule might be required for a high affinity interaction with SH3 domains, a situation without precedent in well-characterized SH3–target interactions. Also of interest is the observation that Nef exhibits differential affinity for different Src family SH3 domains and that this specificity can be altered by mutations at a single site in a loop of the SH3 domain (the RT loop) (Lee et al., 1995). Mutation of Arg-96 to isoleucine in the RT loop of the Fyn SH3 domain converts its interaction with Nef from low affinity ($K_d$ > 20 μM) to high affinity ($K_d$ ≈ 0.38 μM). The affinity of Nef for Fyn (R96I) is comparable with that for the wild-type Hck SH3 domain ($K_d$ ≈ 0.25 μM), which contains an isoleucine at this position. The influence of this isoleucine on Nef binding cannot be readily understood in terms of the interactions seen in the known structures of SH3 domains complexed with peptide ligands (Lee et al., 1995), again suggesting a role for tertiary interactions between Nef and SH3.

We now report the crystal structure, determined at 2.5 Å resolution, of the conserved core of HIV-1 Nef (residues 56–205) in complex with the Fyn(R96I) SH3 domain. In addition to revealing the three-dimensional structure of Nef, our analysis shows that Nef interacts with the SH3 domain via a polyproline type II (PP-II) helix, which includes the PxxP motif. However, in contrast with previous structures of SH3–peptide complexes, the Nef–SH3 interface also includes elements that are distinct from the PP-II helix. Most important of these is a hydrophobic pocket on the surface of Nef that engages the specificity-determining isoleucine residue of the SH3 domain. This pocket is formed by the anti-parallel arrangement of two α helices that follow the PxxP motif in sequence and bracket it in the tertiary structure of Nef. Analysis of the structure of the Nef–SH3 complex adds considerable support to the hypothesis that Nef

functions as an SH3-docking protein and also identifies regions of Nef that are likely to be interaction sites for factors other than the SH3 domain. The structure also provides a template for the design of potential inhibitors of Nef action.

## Results and Discussion

### Definition of Nef Core Region and Structural Analysis

Previous studies using limited proteolysis had suggested that Nef contains two domains: a smaller N-terminal domain (residues 1–57 in HIV-1 NL4-3) and a larger C-terminal domain (residues 58–203) (Freund et al., 1994a, 1994b). The two domains of Nef can be separated in vitro by digestion with proteases, including the HIV protease, which cleaves at a conserved site between residues 57 and 58 (Freund et al., 1994a). Apart from a conserved myristylation motif, the N-terminal domain is polymorphic and highly susceptible to proteolytic degradation, suggesting that it may not have a well-defined fold. The C-terminal domain, in contrast, is highly conserved and has been shown to form a well-defined and relatively stable structure (Shugars et al., 1993; Freund et al., 1994a).

We have shown previously that full-length Nef protein (HIV-1 NL4-3, 206 residues, purified from a bacterial expression system) binds tightly to the SH3 domain of Hck and to a mutant SH3 domain (R96I) of Fyn (Lee et al., 1995). We were unable to crystallize full-length Nef, in the presence or absence of SH3 domains. We therefore utilized a combination of deletion mutagenesis, limited proteolytic digestion, and mass spectrometric analysis (Cohen et al., 1995b) to define a smaller fragment of Nef (residues 39–205) that retained high affinity binding to SH3 domains and readily yielded large crystals of the complex of Nef with Hck SH3. These crystals, however, diffracted only to 6 Å resolution and could not be improved. The Nef construct was then truncated to the highly conserved core (Nef$_{core}$, residues 54–205). This version of Nef yielded crystals with the Hck SH3 domain that diffracted poorly. However, cocrystallization with the Fyn(R96I) SH3 domain resulted in the rapid growth of large crystals of the complex that diffract to 2.8 Å in the laboratory and to 2.5 Å using a synchrotron X-ray source.
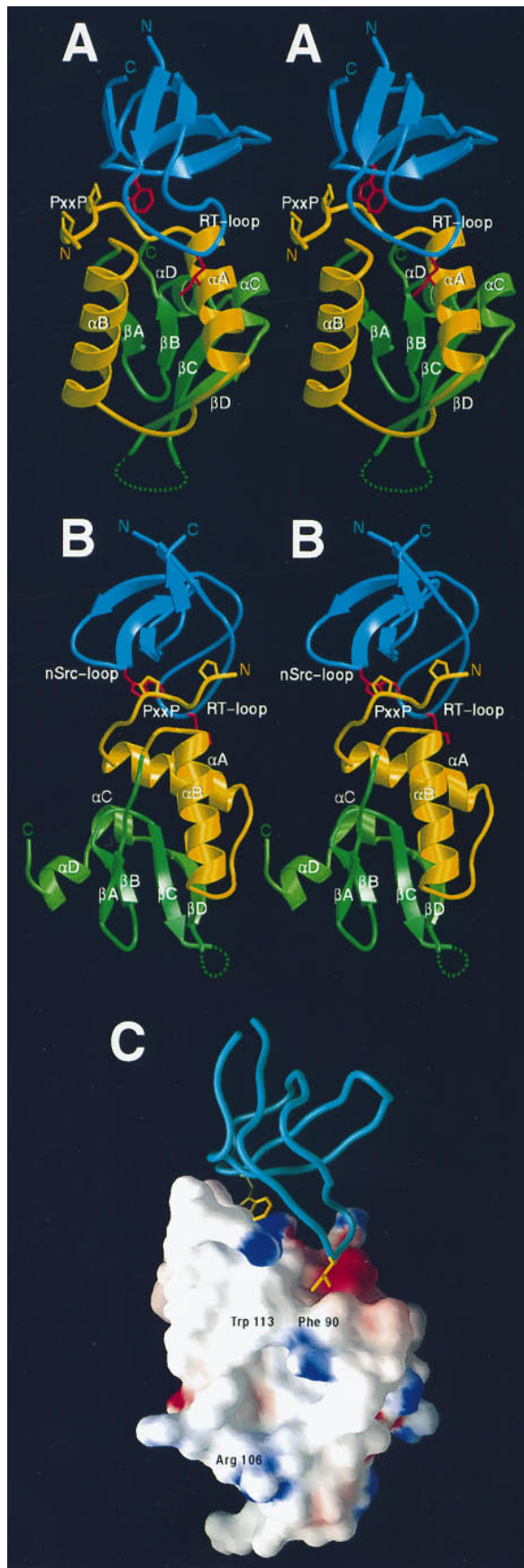
The crystal structure of the Nef$_{core}$–Fyn(R96I) SH3 complex was determined and refined at 2.5 Å resolution using multiwavelength anomalous diffraction (MAD) analysis (Hendrickson, 1991) of a lead derivative for the initial phase determination. The crystals (P6$_5$22; a = b = 107.8 Å, c = 229.1 Å) contain two Nef–SH3 complexes in the asymmetric unit. The current refined model consists of 2635 nonhydrogen protein atoms (including both Nef–SH3 complexes), 99 water molecules, and 2 trimethyl lead molecules. The R value for the model (using data between Bragg spacings of 6.0 and 2.5 Å) is 21.5% (free R value of 28%) (see Table 1). The model for both complexes consists of residues 71–148 and 178–203 of Nef$_{core}$ (Figure 1) and residues 85–141 of the Fyn(R96I) SH3 domain. Two regions of Nef$_{core}$ are disordered in the crystal and are not modeled: the N-terminal 16 residues and 29 residues in a large internal loop (residues 149–177) that is distant from the SH3-binding surface.

The two molecules of Nef in the asymmetric unit are very similar in structure (root-mean-square deviation [rmsd] in Cα positions of 0.7 Å), as are the two SH3 domains (Cα deviation of 0.6 Å). In addition, the structures of the SH3 domains are quite similar to that of uncomplexed wild-type Fyn SH3 (Noble et al., 1993) (rmsd values in Cα positions of 0.45 Å and 0.6 Å, respectively). The intermolecular interfaces of the two Nef–SH3 complexes in the asymmetric unit are also quite similar in general terms. There is, however, a small but significant difference in the relative orientation of the SH3 domain with respect to Nef in the two complexes that appears to be due to differences in crystal packing interactions (see below). The SH3 domain from one complex has a lower average temperature factor (30 Å$^2$) than the other (53 Å$^2$), and the former complex is used for all analysis unless stated. The temperature factors for the Nef molecules in both complexes are similar (31 Å$^2$ and 28 Å$^2$, respectively, for all atoms). The difference in temperature factors of the two SH3 domains may be related to the fact that the one with the higher temperature factors has significantly fewer crystal lattice contacts.

### Structure of Nef$_{core}$

The architecture of Nef$_{core}$ consists of three layers. The N-terminal region forms an outer layer that consists of a PP-II helix (Arg-71 to Arg-77), which contains the PxxP motif, followed by two anti-parallel α helices (αA and αB) that pack against a middle layer of four anti-parallel β strands (Figures 2A and 2B). The C-terminal region consists of two short α helices and packs on the other side of the β strands. The first helical layer forms a contiguous region on the surface of Nef$_{core}$ that is responsible for the entire interaction with SH3 (Figure 2C). The interaction surface is formed by the closed arrangement of the helices. The PP-II helix leads into helix αA and also packs against the C-terminal edge of helix αB. The two α helices are connected by a relatively long linker (ten residues), and although they are in an anti-parallel arrangement, they do not pack closely against each other. Instead, they are separated by approximately 10.5 Å (distance of closest approach of Cα atoms), with their axes inclined by 70°, so as to create a hydrophobic and solvent-accessible crevice between them (Figure 3A). The major portion of this crevice between the helices is unoccupied by the SH3 domain and is separated from the SH3-binding region by two aromatic residues (Trp-113 and Phe-90; see Figure 3A). Conserved side chains that line this crevice are available for potential interactions with other molecules (Figure 3A). The general features of the crystal structure are consistent with the demonstration by nuclear magnetic resonance (NMR) of the presence of two anti-parallel α helices corresponding to αA and αB and the anti-parallel nature of the strand network (Grzesiek et al., 1995).

The four anti-parallel strands that make up the second layer of Nef$_{core}$ are irregular in their architecture. They do not form a contiguous four-stranded β sheet, but are instead separated into two distinct anti-parallel pairs of strands (Figure 3B). Strand βA is part of an extended chain that runs from the C-terminus of helix αB, at Gly-119, to a turn at Val-133. The chain is kinked at a Pro-Asp-Trp sequence (residues 122–124), with the tryptophan side chain being buried in the hydrophobic core

Table 1. Data Collection and Refinement Statistics

Statistics of the Crystallographic Analysis

| Data Set | Resolution (Å) | Reflections Measured/Unique | Completeness (%) Overall/Outer Shell | $R_{merge}$ (%)[a] Overall/Outer Shell | $R_{iso}$[b] |
|---|---|---|---|---|---|
| MAD analysis | | | | | |
| Trimethyl lead acetate[c] | | | | | |
| λ1(0.9552 Å) | 15.0–3.1 | 153,765/14,703 | 99.6/100.0 | 6.8/23.2 | 0.0377 |
| λ2(0.9497 Å) | 15.0–3.1 | 153,710/14,701 | 99.6/100.0 | 6.5/23.6 | — |
| λ3(0.9473 Å) | 15.0–3.1 | 153,506/14,610 | 99.0/99.8 | 7.2/25.0 | 0.0356 |
| λ4(0.9428 Å) | 15.0–3.1 | 153,753/14,696 | 99.6/100 | 7.0/24.6 | 0.0369 |
| Overall MAD figure of merit, 0.34 (15Å–3.2Å) | | | | | |
| MIR analysis | | | | | |
| Native | 30–3.2 | 55,790/10,094 | 74.3/52.0 | 5.7/17.2 | |
| Se-methionine[d] | 30–3.2 | 268,848/13,028 | 97.2/98.5 | 8.0/30.8 | |
| Trimethyl lead acetate[d] | 20–2.5 | 565,661/26,464 | 94.2/84.9 | 6.8/35.8 | |

Refinement Statistics

| | Resolution (Å) | Completeness (%) | R Factor | Free R Factor[e] | Number of Reflections |
|---|---|---|---|---|---|
| Data with F > 2σF | 6.0–2.5 | 80.1 | 0.215 | 0.282 | 20,684 |
| Data with F > 0σF | 6.0–2.5 | 90.2 | 0.235[f] | 0.289[f] | 23,299 |
| Rmsd bond lengths (Å) | 0.010 | | | | |
| Rmsd bond angles (Å) | 1.5 | | | | |
| Rmsd B values (Å²) | 1.4 | | | | |

[a] $R_{merge} = 100 \times \Sigma_h \Sigma_i |I_{h,i} - <I_h>|/\Sigma_h \Sigma_i I_{h,i}$.
[b] $R_{iso} = \Sigma_h |F_{nat,h} - F_{deriv,h}|/\Sigma_h F_{nat,h}$. For MAD analysis, $R_{iso}$ is calculated between data sets at two wavelengths. Wavelength 2 is used as a reference data set ($F_{nat}$) in this calculation, and $F_{deriv}$ refers to data at another wavelength.
[c] Two sites, Brookhaven National Laboratory synchrotron.
[d] Two sites, Cornell High Energy Synchrotron Source.
[e] Free R factor was calculated with 10% of the data.
[f] Note that data with |F| < 2σF were not used in the refinement.

of the molecule. The short βA strand consists of residues 126–128, which each form at least one anti-parallel β-sheet hydrogen bonding interaction with residues in βB, and is terminated by a Pro-Gly-Pro-Gly-Val-Arg-Tyr-Pro sequence that induces a wide bend and irregular conformation in the chain owing to the presence of the three prolines. Only two hydrogen bonds are formed between strands βB and βC. The presence of two strictly conserved prolines, one at position 136 (in βB) and the other at 147 (immediately following βC) appears to hold



Figure 1. Sequence Alignment of Nef_core

The amino acid sequences of the conserved core region of Nef protein from different strains of HIV-1, HIV-2, and SIV are shown. Residue numbers above the sequences correspond to HIV-1 NL4-3. The secondary structural elements of the Nef_core crystal structure are indicated by arrows for strands (labeled βA–βD) and boxes for α helices (labeled αA–αD); the PP-II helix is indicated. A loop connecting βC and βD is disordered in the structure and is indicated as a broken line. Residues involved in the interaction with SH3 are labeled with an asterisk above the sequence. The NL4-3 strain used in this paper (marked by superscripted plus) contains a mutation that replaces Thr-71 with arginine, corresponding to most patient-derived sequences. The sequences shown were obtained from a database at Los Alamos National Laboratory, via internet (http://hiv-web.lanl.gov/) and were selected in an attempt to illustrate the diversity of Nef sequences. The particular HIV-1, HIV-2, and SIV subgroupings shown are as given in the Los Alamos database. The groupings are based on sequence similarity and not on the origin of the virus.

apart the two strands, preventing the formation of a contiguous sheet structure across strands A, B, C, and D (Figure 3B). The paucity of regular hydrogen bonding interactions between the strands, although unusual, is not without precedent. For example, the structure of the C-type lectin domain consists of a number of irregular strands with limited interstrand hydrogen bonding (Weis et al., 1991).

The C-terminal region of $Nef_{core}$ (residues 187–203) only partially covers the distal surface of the β strands, and thus the bulk of the hydrophobic core of the domain is formed between the strands and the N-terminal helices. The irregular architecture of the strands coupled with the spatially separated orientation of αA and αB results in a relatively loose and open appearance to the structure and suggests that the fold of $Nef_{core}$ might not be particularly stable.

**Interaction with the SH3 Domain**
The structure of the Fyn SH3 domain has been described previously (Noble et al., 1993), and the structure of the Fyn(R96I) SH3 domain seen here is essentially unchanged. The β barrel structure of the SH3 domain presents an array of conserved hydrophobic side chains that are spaced appropriately for interaction with polyproline helices (Figure 4C). Two loops that abut this interaction surface are of particular interest in terms of SH3 specificity: the so-called RT-Src or RT loop (between the first and second strands of the SH3 domain) and the n-Src loop (between the second and third strands). The historical nomenclature for these SH3 loops refers to critical arginine and threonine residues in the RT loop in Src and to insertions in the n-Src loop in neuronal forms of Src. The RT loop plays a key role in the interaction with Nef, while the n-Src loop does not.

Residues 71–77 of Nef form a left-handed PP-II helix that spans the strictly conserved PxxP motif. The PP-II helix has side chains emanating in three directions, two of which are utilized for interactions with the SH3 domain

Figure 2. Structure of Nef–SH3 Complex

(A and B) Stereo diagrams of the polypeptide backbones of $Nef_{core}$ and Fyn(R96I) SH3. The N-terminal helical layer of $Nef_{core}$ (residues 71–120), which forms the SH3 interaction surface, is colored yellow. The rest of $Nef_{core}$ (residues 121–203) is colored green. The disordered loop (residues 149–178) between βC and βD is indicated as a dotted line. The Fyn(R96I) SH3 domain is in blue. Also shown are the side chains of the conserved tryptophan of SH3 (residue 119, in red), the specificity-conferring isoleucine of SH3 (residue 96, in red), and the two prolines that define the PxxP motif of Nef (residues 72 and 75, in yellow). The views in (A) and (B) are approximately orthogonal. The figure was prepared using MOLSCRIPT (Kraulis, 1991) and Raster3D (Bacon and Anderson, 1988).
(C) The molecular surface of $Nef_{core}$, with Fyn(R96I) SH3. The local electrostatic potential of $Nef_{core}$ was calculated in the absence of the SH3 domain using GRASP (Nicholls et al., 1991). The molecular surface is colored according to the local electrostatic potential, with colors ranging from dark blue (most positive region) to deep red (most negative) through white (neutral). The SH3 domain is shown as a blue tube. The side chains of Trp-119 and Ile-96 of SH3 are shown in yellow. Trp-113 and Phe-90 of Nef separate the binding pocket for Ile-96 of SH3 from the hydrophobic crevice that is available for potential interaction with other molecules. Arg-106 of Nef, located at the lower left edge of the crevice, is implicated in the association of Nef with a Ser kinase activity (Sawai et al., 1995).
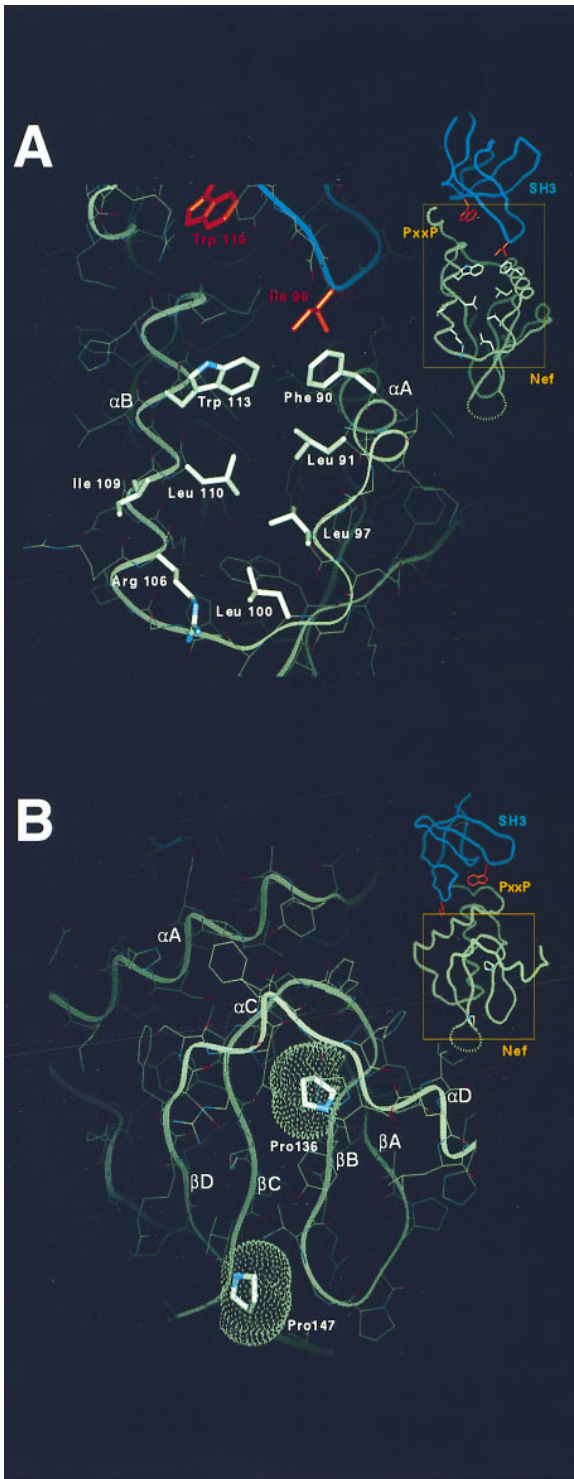
(Figure 4). PP-II helices can bind to SH3 domains in two orientations, "plus" and "minus," with the particular choice of direction being dictated by electrostatic complementarity and by steric restrictions set by the presence of nonproline residues on one or the other interacting edge of the PP-II helix (Feng et al., 1994; Lim et al., 1994). The Nef PP-II helix interacts with the SH3 domain in the minus orientation, and the interface with the SH3 domain is strikingly similar to that seen in the structures of similarly oriented peptides bound to the SH3 domains of Sem5, Grb2, Src, and Crk (Lim et al., 1994; Feng et al., 1994; Terasawa et al., 1994; Wu et al., 1995; Goudreau et al., 1994). In the following discussion, we compare the Nef PP-II–SH3 interaction with the interaction between the N-terminal SH3 domain of c-Crk and a peptide corresponding to a sequence in the guanine–nucleotide exchange factor Sos (Wu et al., 1995). Similar features are seen in structures of Sem5, Grb2, and Src SH3 domains complexed with peptides. For consistency, we adopt the notation used previously and refer to binding sites for the PP-II helix as $P_{-1}$, $P_0$, $P_{+1}$, and so forth (Lim et al., 1994), where Val-74 of Nef occupies the $P_0$ position. Note that in the minus orientation seen here, the numbering of these sites runs counter to the direction of the polypeptide chain of the PP-II helix of Nef.

One edge of the PP-II helix of Nef contains the two residues that define the PxxP motif, Pro-72 and Pro-75. These occupy the $P_{-1}$ and $P_{+2}$ sites on the SH3 domain and pack against conserved hydrophobic side chains (Tyr-91, Trp-119, Pro-134, and Tyr-137 of SH3; Figures 4A and 4C). The other edge of the PP-II helix that interacts with the SH3 includes three nonproline residues (Arg-71, Val-74, and Arg-77). The arginine residues provide hydrophobic, hydrogen bonding, and electrostatic interactions with the SH3 domain. Arg-77 is strictly conserved in Nef sequences (Figure 1) and is critical to the integrity of the interface, since it is involved in the formation of an extensive network of interactions with other components of the Nef structure and with the SH3 domain (Figure 5B). This side chain stacks closely against a face of the Trp-119 side chain of SH3 and forms a salt bridge with a conserved acidic residue (Asp-100) in the RT loop of SH3. Similar ion pairing interactions have been observed in many SH3–peptide complexes. The N-terminal Arg-71 of Nef is relatively poorly ordered, but forms a hydrogen bond via its Nζ atom with the hydroxyl group of Tyr-137 and may also contribute to electrostatic complementarity, since it is in the vicinity of two acidic residues (Asp-92 and Glu-94) of the SH3 domain. Val-74 of Nef occupies the central $P_0$ binding

Figure 3. Architecture of Nef

(A) The spacing between the two helices, αA and αB, and the loop connecting them is illustrated. A hydrophobic crevice is formed between the two helices. The crevice is bordered by eight conserved residues and is separated from the SH3 interaction surface by the side chains of two aromatic residues (Trp-113 and Phe-90). Arg-106, which has been found to be essential for the association of Nef with a Ser kinase activity (Sawai et al., 1995), is located at one edge of this crevice. The insert shows a ribbon diagram of the Nef–SH3 complex in the same orientation. The boxed region is

shown in detail in the main figure. The SH3 domain and Nef$_{core}$ are shown in dark blue and in green, respectively. The conserved tryptophan (residue 119) and the specificity-conferring isoleucine (residue 96) of the Fyn(R96I) SH3 domain (shown in red) are provided as landmarks.

(B) The irregular architecture of the four anti-parallel strands (βA–βD) of Nef$_{core}$. Two strictly conserved prolines (residues 136 and 147) hold apart the two hairpins, and the van der Waals surfaces of these two prolines are shown as dotted surfaces. The insert shows a ribbon drawing of the Nef$_{core}$–Fyn(R96I) complex. The boxed region is shown in detail in the main figure.
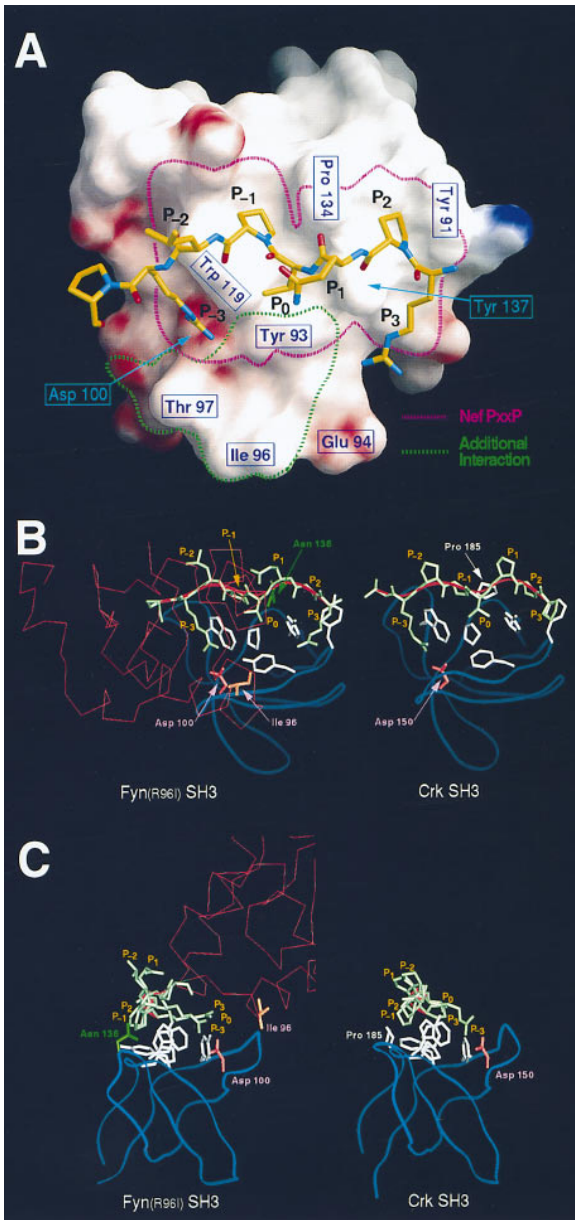
Figure 4. Comparison of the Nef–SH3 and Peptide–Crk SH3 Interfaces

(A) The footprint of Nef on the surface of the Fyn(R96I) SH3 domain. The region on the SH3 surface that is occluded by the Nef PP-II helix (including the PxxP motif) is outlined in pink. An additional region on the SH3 surface that is occluded by other elements of Nef is marked with a green dotted line. Tyr-93 of the SH3 domain is partially covered by Nef PxxP motif and is completely buried when the rest of the Nef$_{core}$ is included. The surface is colored according to the local electrostatic potential, calculated in the absence of Nef$_{core}$ using GRASP (Nicholls et al., 1991). Surface colors range from dark blue (most positive region) to deep red (most negative) through white (neutral). The Nef PP-II helix is shown as a stick figure, with atoms colored as follows: carbon, yellow; nitrogen, blue; oxygen, red.

(B and C) Comparison of Nef PP-II helix interacting with Fyn(R96I) SH3 (left) with the Sos peptide–Crk SH3 interaction (right) (Wu et al., 1995). In (B), the view is approximately perpendicular to the SH3-binding surface. The polypeptide backbones of the SH3 domains are shown as blue ribbons, and the conserved hydrophobic residues

on the interaction surfaces of the SH3 domains are colored white. The PP-II helices are shown in green, with the polypeptide backbone of the helices indicated as red ribbons. To the left, the rest of Nef$_{core}$ is shown as a red Cα backbone trace. Ile-96 of the Fyn(R96I) SH3 domain is shown in red, as is Asp-100. The view in (C) is approximately orthogonal to that in (B) and emphasizes the 3-fold pseudo-symmetry of the PP-II helices formed by the PxxP motifs. Two of the three edges of the PP-II helices pack against conserved hydrophobic residues (in white) on the surface of the SH3 domains. In the Nef–SH3 complex (left), Asn-136 of the Fyn(R96I) SH3 domain forms a hydrogen bond with the backbone of the PP-II helix of Nef. Although Crk has a proline in the corresponding position (right), other SH3 domains have glutamine (Lim et al., 1994). The view shown is from the C-terminus of the PP-II helix in both cases.
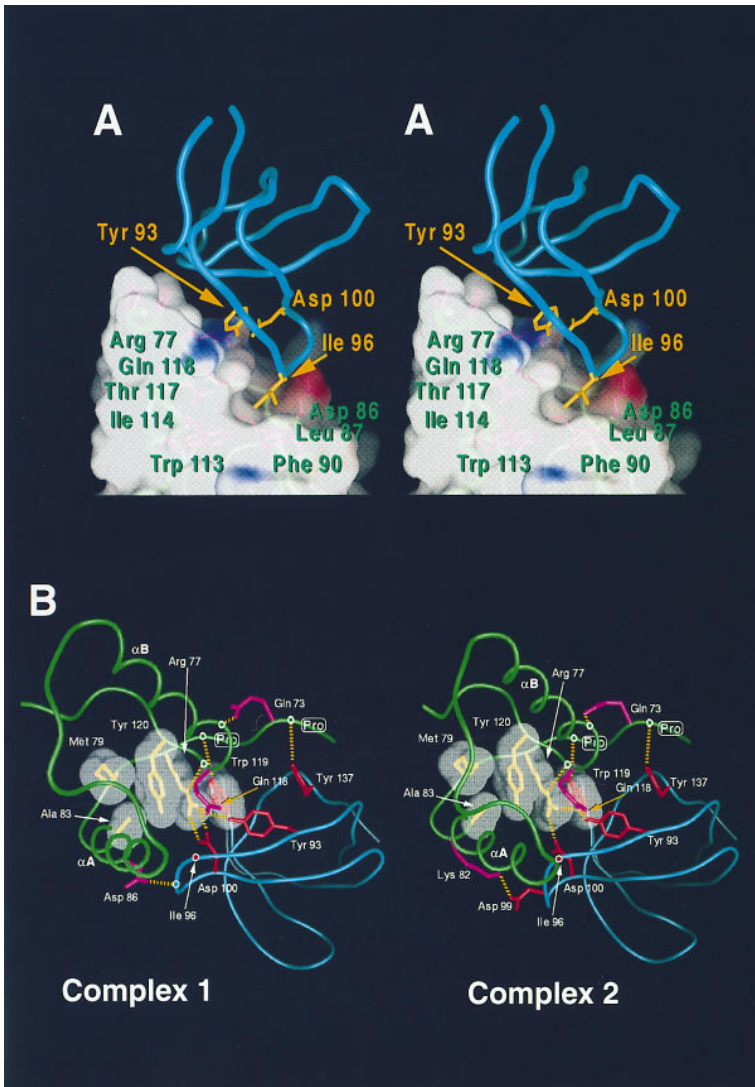
site and packs against Tyr-93, Trp-119, and Tyr-137 side chains of SH3. Val-74 is highly conserved in Nef sequences and is completely buried at the interface owing to tertiary interactions in the Nef protein.

Pro-72 and Pro-75 are strictly conserved in all Nef sequences and are essential for the enhancement by Nef of viral replication in vitro (Saksela et al., 1995). The critical role for these two residues in Nef function correlates with their central position at the Nef–SH3 interface. In contrast, prolines at positions 69 and 78 are not as highly conserved among primate immunodeficiency viruses (Figure 1) and are dispensable for the binding to SH3 domains (Lee et al., 1995). Pro-69 is part of the N-terminal disordered region of Nef$_{core}$ and is not modeled in the crystal structure. Pro-78 does not interact directly with the SH3 domain, but instead plays a structural role in the recognition by causing a kink in the loop connecting the PP-II helix to helix αB. The side chain of Tyr-120, which is part of the network of tertiary interactions at the interface (Figure 5B), packs against the backbone of Pro-78.

There is remarkably close correspondence between the way in which the PP-II helix of Nef docks on the SH3 domain and the mode of interaction of peptide ligands with SH3 domains (Figures 4B and 4C). If the SH3 domains of the Nef–SH3 complex and the Crk–peptide complex are superimposed, the average deviation in the positions of the Cα atoms of the two PP-II helices is 1.1 Å. The similarity in the general disposition of the Nef PP-II helix on the SH3 surface with that of peptide ligands is also emphasized by the fact that very similar hydrogen bonding interactions between the peptide and the SH3 domain are seen in the two cases. Hydrogen bonds between the backbone of the PP-II helix of Nef and the side chains of Trp-119 and Tyr-137 of the Fyn(R96I) SH3 domain are similar to those seen in peptide complexes of Crk, Grb2, and Sem5. Asn-136 of Fyn SH3 forms a hydrogen bond to the backbone of the PP-II helix (Figures 4B and 4C). Many SH3 domains, including Grb2, have a glutamine at this position, and a similar hydrogen bonding interaction is found in the Grb2–peptide complex (Lim et al., 1994).

### Tertiary Interactions between Nef$_{core}$ and SH3
Unlike in SH3–peptide interactions, the Nef PxxP motif is presented in the context of a folded protein that contributes additional elements to the binding interface. Consequently, the interaction surface of Nef with the SH3

Figure 5. Tertiary Interactions between Nef$_{core}$ and Fyn(R96I) SH3 Domain

(A) Molecular surface of Nef, showing the binding site for the isoleucine side chain of the SH3 domain.

(B) Comparison of the interactions in the two complexes in the crystal. The polypeptide backbones of Nef and the SH3 domain are shown as green and blue tubes, respectively. Side chains of Nef are shown in pink and in yellow (displayed under their respective molecular surfaces). SH3 side chains are shown in red. Hydrogen bonding interactions are shown as dashed lines. Hydrogen bonds to backbone positions are indicated by the placement of white circles along the backbone ribbon. For clarity, the side chain of Ile-96 is not shown, and instead the Cα position of this residue is indicated with a red circle. The structure on the left is the complex that is the focus of the major part of the discussion in the text. The structure on the right is that of the second independent complex in the crystal. Note the slight change in the relative orientation of the Nef and SH3 components of the complex (see text). The side chain of Asp-86 forms a hydrogen bond with Thr-97 in the RT loop of the second complex. For clarity, this interaction is not shown.

domain is larger than for an isolated peptide. The total accessible surface area on Nef and on the SH3 domain that is buried upon formation of the complex is ~1200 Å² (calculated using a probe of radius 1.4 Å), with about 600 Å² buried on each partner. In comparison, if the PP-II helix alone of Nef is considered, the total buried surface area is ~780 Å², with ~390 Å² buried on the SH3 domain. The increase in interaction area between the SH3 domain and Nef relative to the core interaction of the PP-II helix is due to contributions from the two helices αA and αB and adjacent residues in Nef and from the RT loop in the SH3 domain (Figure 4A).

The PP-II helix of Nef interacts with the rest of Nef as well as with the SH3 domain. The total accessible surface area of the Nef PP-II helix, considered separately from the rest of the protein, is ~1200 Å². In the Nef–SH3 complex, approximately a third of the surface area of the PP-II helix is buried by the SH3 domain and a third by the rest of the Nef protein. The main interaction of the PP-II helix with other elements of Nef involves the C-terminal region of helix αB and the loop immediately following (Figure 5B). The side chain of Gln-73 in the

PxxP motif is hydrogen bonded to the backbone of αB. Three other hydrogen bonding interactions between the PxxP motif and the C-terminal region of αB are likely to be important for stabilizing the position of Arg-77, a critical component of the Nef–SH3 interface. The backbone carbonyl groups of residues 118 and 119 are hydrogen bonded to the Nζ atom of Arg-77 and the backbone amide of Leu-76, respectively. The conformation adopted by these two consecutive carbonyl groups is made possible by the presence of a strictly conserved glycine at position 119 of Nef (see Figure 1). Finally, the amide nitrogen at position 121 of Nef hydrogen bonds to the carbonyl group of Arg-77.

In the Nef–SH3 complex, the RT loop of the SH3 domain extends over the surface of Nef, such that the side chain of Ile-96 of SH3 is inserted into a pocket formed between helices αA and αB of Nef (Figures 2A, 3A, and 5A). The interaction of the RT loop with Nef thus involves a hydrophobic anchor point, the isoleucine side chain at position 96, which packs against the conserved side chains of Leu-87, Phe-90, Trp-113, and Ile-114 of Nef. The rest of the Nef–SH3 interface is remarkably polar,

with the exception of the two proline and the valine residues of the PP-II helix.

The polar nature of the central region of the interface results from the formation of a network of interconnecting hydrogen bonds between Nef and the SH3 domain. A notable feature of this network is the role played by Arg-77 of the PP-II helix of Nef. In the Nef–SH3 complex, the interaction of Arg-77 with Asp-100 is likely to be strengthened by the formation of stacking interactions between Arg-77 and a conserved tryptophan side chain of the SH3 domain (Trp-119) on one side and the side chain of Tyr-120 of Nef on the other. Tyr-120 is positioned by packing against Met-79 and Ala-83 of Nef. Asp-100 of SH3 is also hydrogen bonded to Gln-118 of Nef, which is at the C-terminus of helix $\alpha$B. Gln-118 is hydrogen bonded to the hydroxyl group of Tyr-93 of the SH3 domain, which interacts with the valine side chain at position $P_0$ of the PP-II helix of Nef. The buttressing of the interaction of Arg-77 with Asp-100, in the RT loop, has an additional significance in the Nef–SH3 complex, since it serves to position the Ile-96 side chain that is also in the RT loop and is involved in the hydrophobic interaction with the crevice on the surface of Nef.

Most of the SH3 residues involved in the hydrogen bonding network at the Nef–SH3 interface are highly conserved in Src family SH3 domains and are therefore unlikely to play a role in determining the specificity of the interaction. However, they function to place the RT loop in a defined orientation on the Nef-binding surface. In addition to being highly variable in its sequence, the RT loop of SH3 domains is a highly flexible element (e.g., Gosser et al., 1995), and the hydrogen bonding network at the Nef–SH3 interface is likely to localize the RT loop, allowing "readout" by the Nef surface of the specificity-determining residues of the SH3. These interactions clearly lead to quite high specificity, with a greater than 100-fold selectivity over closely related SH3 domains (Lee et al., 1995). The low affinity of wild-type Fyn SH3, with an arginine at position 96, is readily understood given the hydrophobic nature of the binding site for Ile-96 in the mutant.

Despite the similarity between the SH3 interactions of the PP-II helix of Nef and peptide ligands of SH3 domains, isolated peptides corresponding to this region of Nef do not bind with high affinity to SH3 domains. For example, the 12-mer peptide PVRPQVPLRPMT, which encompasses the PxxP motif of Nef, binds to the Hck SH3 domain with a $K_d$ of 91 $\mu$M (Lee et al., 1995). In contrast, the peptide PPPVPPRRRR (derived from Sos), used in the comparative illustrations, binds to the Crk SH3 domain with a $K_d$ of 5.2 $\mu$M (Knudsen et al., 1995). Part of the reduction of binding affinity of the Nef PxxP peptide is likely to be due to the presence of nonproline residues at the nonbinding edge of the PP-II helix (glutamine at $P_{-1}$ and leucine at position $P_{-2}$). In the case of the isolated peptide binding to the SH3 domain, these residues do not contribute to the binding interface and are likely to increase the entropic cost of forming the PP-II helix. The intact Nef protein binds more than 300 times more tightly to the SH3 domain than the isolated peptide, indicating that the additional interactions described here compensate for these destabilizing factors.

## Flexibility of the Nef–SH3 Interface

There are two Nef–SH3 complexes in the asymmetric unit of the crystal, and these have different crystal packing interactions with the lattice. The structures of the SH3 and Nef domains are similar in the two complexes, but differ in the relative orientation of Nef and SH3 (Figure 5). The PP-II helix of one of the two Nef molecules is rotated by about 15° with respect to the orientation of the other. However, the position of the PP-II helix with respect to the SH3 domain is essentially unchanged (the SH3 domain and the PP-II helix move as one unit), which results in a 15° rotation of Nef (excluding the PP-II helix) with respect to the SH3 domain, pivoted about a point close to the C-terminal end of the PP-II helix.

The net effect of the conformational change is that the SH3 domain and Nef are tipped such that the isoleucine side chain of the SH3 domain in the second complex is more buried in the binding pocket on Nef. All of the interactions described for the first domain are generally preserved in the second complex, although some of the details differ because side chain positions have changed by 1–2 Å owing to the intermolecular rotation (Figure 5B). The most extreme difference involves the interaction of helix $\alpha$A with the RT loop of the SH3 domain. In the first complex, the side chain of Asp-86 (strictly conserved in the Nef sequences shown in Figure 1) hydrogen bonds with the backbone of the RT loop. This interaction is replaced in the second complex by a hydrogen between Asp-86 and the side chain of Thr-97 of the SH3 and an additional ion pairing interaction between the well-ordered side chains of Lys-82 of Nef and Asp-99 in the RT loop of the SH3 domain (Figure 5B).

This conformational difference emphasizes an essential feature of the Nef–SH3 interface. Rather than a rigid interdigitation of hydrophobic side chains, the polar nature of the Nef–SH3 interaction results in some degree of flexibility at the interface. In particular, adjustments in the positions of hydrogen-bonding groups at the interface may be assisted by the participation of water molecules in the network of interactions. Although water molecules are observed at certain positions at each of the interfaces, a detailed analysis of the role of these waters awaits the measurement of more accurate X-ray data at higher resolution.

## Sequence Variation in Nef$_{core}$

The Nef sequences shown in Figure 1 are representative of the range of sequence diversity observed in HIV-1, HIV-2, and SIV. For the region corresponding to the ordered structure in the crystal (residues 71–203, excluding the disordered loop between $\beta$C and $\beta$D), the sequences in the HIV-1 subgrouping are highly conserved. The Nef variant used here (HIV NL4-3) is 81% identical to the HIV MAL sequence, the most distant in the HIV-1 grouping. Sequences in the HIV-2 and SIV groupings are more divergent, with sequence identities with respect to HIV NL4-3 of 57% for HIV-2 EHOA and 49% for SIV AGM155, for example. However, substitutions at most positions across Nef$_{core}$ are highly conservative (except in the disordered $\beta$C–$\beta$D loop), indicating that the three-dimensional structure reported here will be a reasonable model for all Nef sequences.

There are 25 positions that are conserved without exception in all the sequences shown in Figure 1. The strictly conserved residues that do not appear to have a major structural role fall into two categories. Five are involved in interactions with the SH3 domain (Pro-72, Pro-75, Leu-76, Arg-77, and Asp-86). The three other strictly conserved residues, Arg-106, Ile-109, and Leu-110, are located on the edge of the crevice between helices $\alpha$A and $\alpha$B (Figure 3A). The hydrophobic nature of the side chains lining this crevice is conserved in all Nef sequences (Figure 1), and Arg-106 has been implicated in the association of Nef with Ser kinase activity (Sawai et al., 1995). The arrangement of hydrophobic side chains seen here is strongly suggestive of a binding site for a ligand (Figure 3A).

## Conclusions

The current paradigm for target recognition by SH3 domains focuses on the binding of PxxP motifs and adjacent residues by the SH3 domain. The adoption of the PP-II conformation by SH3-binding sites is an effective solution to the problem of accomplishing molecular recognition within the limitations imposed by the relatively small surface area of the SH3 domain. Previous studies on SH3–peptide interactions have shown how specificity can be achieved by the utilization of residues that are adjacent to the PxxP motif (Feng et al., 1995). The analysis of the Nef–SH3 interaction illustrates a mechanism by which the repertoire of SH3-binding specificity can be extended by presenting the polyproline helix within the context of a folded protein.

Although the particular SH3 domains that are the natural targets of Nef are unknown, the striking congruence between the modes of interaction of SH3 domains with Nef and with peptide ligands lends strong support to the idea that the PxxP motif of Nef has indeed evolved to mediate functional interactions with SH3 domains. However, the physiologically relevant target of Nef could well be an as yet unidentified SH3 domain. Nevertheless, the fact that the SH3-interacting elements defined by the structural analysis are highly conserved in Nef sequences suggests that analysis of the structure described here will be useful in terms of considering general mechanisms for understanding and inhibiting the interaction of Nef with SH3 domains. While this paper was under review, the solution structure of Nef$_{core}$, determined by NMR, was reported (Grzesiek et al., 1996). The general nature of the protein fold in solution is the same as that reported here in the SH3 complex. The NMR analysis shows that the PxxP motif of Nef adopts a PP-II helix in the absence of the SH3 domain.

The importance of Nef for the virulence of HIV-1 is now well established, and the critical role played by the PxxP motif in enhancing viral replication suggests that blocking the interaction of Nef with SH3 domains is likely to interfere with the viral life cycle. In this regard, one intriguing aspect of the structure is the prominent solvent-accessible hydrophobic crevice formed between helices $\alpha$A and $\alpha$B. This crevice is occupied at one end by the specificity-determining isoleucine side chain of the SH3 domain, but is otherwise vacant in the structure of the complex. Compounds that bind to this cavity are likely to disrupt the interaction of Nef with the SH3 domain and possibly with other molecular partners, and the design or discovery of such compounds would likely lead to interesting insights into the mechanism of Nef action, with potential therapeutic implications.

## Experimental Procedures

### Protein Expression and Purification

Polymerase chain reaction (PCR) was used to amplify the core region (residues 54–205) of Nef from HIV-1 NL4-3 (referred to as Nef$_{core}$). A threonine to arginine mutation was introduced at residue 71 to mimic the sequence of most *nef* alleles obtained directly from patients (Shugars et al., 1993; Huang et al., 1995). Nef$_{core}$ was cloned into the pGEX-2T expression vector (Pharmacia), which was modified (C.-H. L., unpublished data) so that the linker between the glutathione S-transferase (GST)-coding region and the cloning site for the protein of interest included a cleavage site for the highly specific tobacco etch virus (Tev) protease (GIBCO). Expression and purification of the GST–Nef$_{core}$ fusion protein in Escherichia coli (strain K12 PR 745; New England Biolabs) was carried out as suggested by Pharmacia. After elution from glutathione–Sepharose beads (Pharmacia), Nef$_{core}$ was cleaved from the fusion protein by Tev protease. Utilization of Tev protease resulted in the production of Nef$_{core}$ with an additional four residues at the N-terminus and avoided problems of nonspecific cleavage that had been observed when using thrombin. Nef$_{core}$ was purified using Q Sepharose, glutathione–Sepharose, and Superdex75 Hiload 16/60 columns on an FPLC system (Pharmacia). The protein was concentrated to 40 mg/ml by ultrafiltration (Amicon). Approximately 36 mg of purified Nef$_{core}$ was obtained from 18 l of culture. Se-methionine-labeled Nef$_{core}$ was purified using similar procedures as for native protein. The identity of the protein was confirmed by mass spectrometry.

The Hck SH3 domain was purified as described previously (Lee et al., 1995). To produce Fyn(R96I) SH3 domain, cDNA encoding the SH3 domain of Fyn(R96I) was amplified by PCR using the pGEX–Fyn(R96I) construct (Lee et al., 1995) as template. The amplified DNA fragment was subcloned into an expression vector, pET3a (Novagen) through NdeI and BamHI sites. Expression of the Fyn (R96I) SH3 domain using the resulting plasmid was performed according to the protocol provided by the supplier of the pET expression system (Novagen). Protein was purified using standard chromatography techniques, including a DEAE Fast Flow column, a Q Sepharose Fast Flow column, a Phenyl Sepharose (high performance) column, and a Superdex75 Hiload 16/60 column on an FPLC system (Pharmacia). The protein was concentrated to 20 mg/ml by ultrafiltration (Amicon). For each purification, 12 l of culture was typically used, and the final recovery of purified Fyn(R96I) SH3 domain was ~24 mg.

### Crystallization and Data Collection

Nef$_{core}$ and Fyn(R96I) SH3 were mixed in a 1:1 molar ratio and dialyzed against a buffer containing 10 mM Tris (pH 7.5), 50 mM KCl, and 2 mM DTT. Crystallization conditions were scanned using the hanging-drop method. Crystals of the complex (approximate dimensions $0.2 \times 0.2 \times 0.1$ mm$^3$) were obtained overnight with ammonium sulfate as the precipitant (1 M) and Tris buffer (100 mM, pH 9.0) at 4°C. The crystals are hexagonal (P6$_5$22; a = 107.8, c = 228.5) and diffract to Bragg spacings of 2.8 Å using an in-house X-ray source.

All diffraction data were measured from crystals cooled to 100 K. Crystals were flash frozen in a stream of N$_2$ (for in-house data collection) or in liquid propane (for data collection at Cornell High Energy Synchrotron Source [CHESS] and Brookhaven National Laboratory synchrotrons) after soaking serially in mother liquor (1.2 M ammonium sulfate, 100 mM Tris buffer [pH 9.0]) containing 5%–30% glycerol. X-ray data for MIR analysis were collected on a Rigaku RAXIS IIC area detector mounted on a Rigaku RU200 X-ray generator (Molecular Structure Corporation, USA) and the A1 beamline at CHESS. MAD data were collected from a single frozen crystal derivatized with 30 mM of trimethyl lead acetate at the National Synchrotron Light Source (Brookhaven National Laboratory) using

beamline X4A. All data were processed using program DENZO and SCALEPACK (Z. Otwinowski and W. Minor).

## Phase Determination

Although several heavy atom derivatives were obtained, severe non-isomorphism between native and derivative crystals prevented the determination of accurate phases by multiple isomorphous replacement. Crystals soaked in solutions containing 30 mM of trimethyl lead acetate yielded a derivative with a strong anomalous diffraction signal ($9\sigma$ peaks in the Harker section of an anomalous difference Patterson map at 3.0 Å resolution, calculated using data measured at the A1 beamline at CHESS, at a wavelength of 0.92 Å). Isomorphous difference Patterson maps contained no interpretable peaks, indicating nonisomorphism.

Phases were determined by carrying out a MAD experiment on the lead derivative. For MAD data collection, a single crystal was derivatized using trimethyl lead and was mounted, after flash freezing, with the c* axis aligned along the rotation axis and perpendicular to the X-ray beam to allow the near simultaneous recording of Bijvoet pairs of reflection. Data collection at four wavelengths near the lead absorption edge (Table 1) were recorded on image plates, digitized with a Fuji scanner, and processed with DENZO and SCALEPACK. Heavy atom parameters were refined and phases were calculated using the program MLPHARE (Z. Otwinowski). Phases calculated at 3.2 Å resolution using only MAD data yielded an interpretable electron density map, which was further improved by solvent flattening and histogram matching using SQUASH (Zhang and Main, 1990). The handedness of the $\alpha$ helices provided definite confirmation of the space group assignment.

## Model Building and Refinement

There are two Nef$_{core}$–SH3 complexes in the asymmetric unit of the crystal. A noncrystallographic 2-fold symmetry operator that relates two complexes in the asymmetric unit was identified by the positions of equivalent helices and heavy atoms. It was evident from the original electron density map that the relative position of the SH3 domain with respect to Nef$_{core}$ is slightly different between the two complexes. Two symmetry operators that relate the two Nef and SH3 molecules, respectively, were therefore used for all subsequent real space density averaging (RAVE, part of the O package) as well for the application of noncrystallographic symmetry restraints during refinement. The 2-fold averaged electron density map (Figure 6A) based on MAD phases was of good quality and allowed a model to be built unambiguously, using program O (Jones et al., 1991). The Fyn SH3 domain structure (Noble et al., 1993) was fit into the averaged electron density map. The sequence assignment for Nef$_{core}$ was quite straightforward, since it has a relatively high aromatic content (12.5% compared with 8.4% on average; see Figures 6A and 6B). The positions of two methionine residues in the asymmetric unit (Met-79) were confirmed in a difference electron density map using X-ray data for a Se-methionine derivative (Met-173 is in a disordered region of the structure and is not observed).

Crystals that have been derivatized using trimethyl lead diffract somewhat better than unmodified crystals, and data collected for the lead derivative were used in all the analysis. The trimethyl lead molecules are bound at crystal contact sites and are distant from the Nef–SH3 interface. The model was refined using X-PLOR (Brünger, 1992), initially using data collected during the MAD analysis. The free R value (Brünger, 1993) was used to monitor all stages of the refinement. Noncrystallographic symmetry restraints (separately for Nef$_{core}$ and for the SH3 domain) were initially applied to the two complexes, except for a small number of residues at the interface between Nef$_{core}$ and SH3. The refinement was later extended to 2.5 Å using data collected at CHESS (Table 1). Finally, the noncrystallographic symmetry restraints were released, and two complexes were allowed to refine independently. Well-ordered solvent molecules were included at this stage, and tightly restrained individual isotropic B factors were refined. The refinement proceeded smoothly, without the utilization of simulated annealing refinement.

The statistics for data collection, phase determination, and refinement are given in Table 1. The working R value is 21.5%, using data between 6.0 and 2.5 Å (20,684 reflections), and the free R value (10% of the data) is 28% for final model using reflections with I/$\sigma$I >
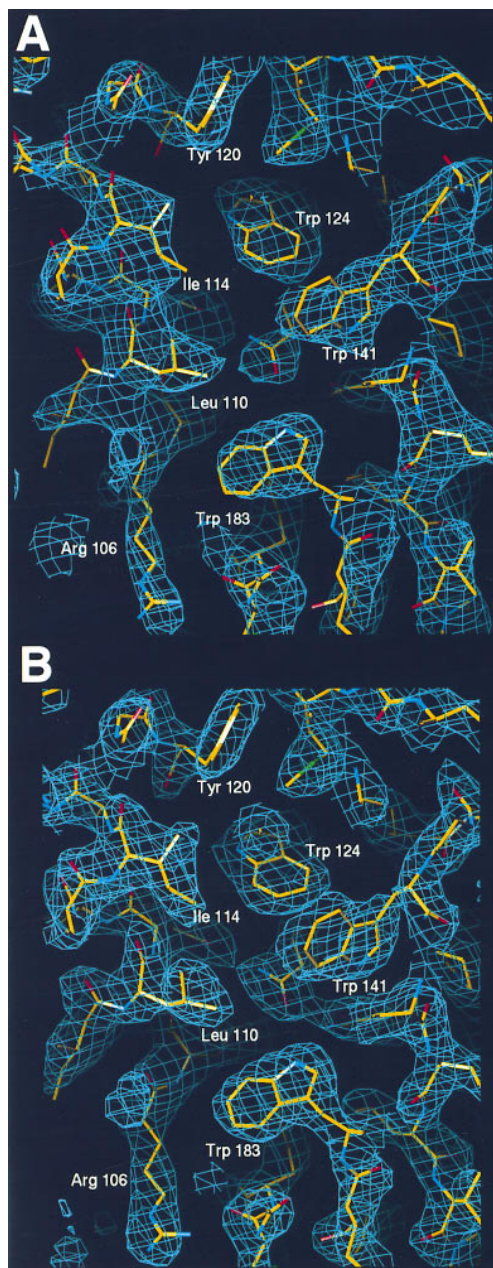


Figure 6. Electron Density Maps in a Region of the Hydrophobic Core of Nef$_{core}$

(A) Electron density map at 3.2 Å resolution, calculated using experimental MAD phases.

(B) Electron density map at 2.5 Å resolution, using phases calculated from the refined model. In (A), the electron density map is calculated using experimentally observed amplitude and phases obtained from the MAD analysis and then modified by solvent leveling and 2-fold real space density averaging. In (B), the electron density map was calculated using coefficients $(2|F_{obs}|-|F_{cal}|)exp(-i\alpha_c)$, where $F_{obs}$ is the observed structure factor amplitude and $F_{cal}$ and $\alpha_c$ are the amplitude and phase calculated from the current model. Blue lines indicate electron density at the 1.5$\sigma$ level. The protein atoms are shown in stick representation, with atoms colored as in Figure 4A.

2.0. The current model includes two complexes of Nef$_{core}$–Fyn(R96I) SH3 domain (residues 71–148 and residues 179–203 of Nef and residues 85–131 of Fyn[R96I] SH3 domain), 99 water molecules, and

2 trimethyl lead molecules. No electron density is present for 16 residues at the N-terminus of Nef$_{core}$, for 29 residues in a loop on the side of Nef$_{core}$ distal to the SH3-binding surface (residues 149–177), and for 2 residues at the C-terminus of Nef$_{core}$. Residues 85–131 of the Fyn(R96I) SH3 domain are included in the model. The average temperature factor for protein atoms is 34 Å$^2$. Although the two Nef$_{core}$–SH3 complexes are similar in general terms, their mutual orientations are slightly different (see main text). One of the SH3 domains exhibits higher temperature factors than the other components of the molecular model (the average temperature factor for this SH3 domain is 53 Å$^2$, compared with 30.0 Å$^2$ for the other SH3 domain and 31 Å$^2$ and 28 Å$^2$ for the two Nef$_{core}$ molecules). The complex with the lower temperature factors is more reliable and is used for all analysis unless stated otherwise. Coordinates will be deposited in the Brookhaven Protein Data Bank.

## References

Bacon, D., and Anderson, W.F. (1988). A fast algorithm for rendering space-filling molecule pictures. J. Mol. Graph. *6*, 219–220.

Bolen, J.B. (1993). Nonreceptor tyrosine protein kinases. Oncogene *8*, 2025–2031.

Brünger, A.T. (1992). X-PLOR (Version 3.1), Manual (New Haven, Connecticut: The Howard Hughes Medical Institute and Department of Molecular Biophysics and Biochemistry, Yale University).

Brünger, A.T. (1993). Assessment of phase accuracy by cross validation: the free R value. Methods and applications. Acta Cryst. *D49*, 24–36.

Cohen, G.B., Ren, R., and Baltimore, D. (1995a). Modular binding domains in signal transduction proteins. Cell *80*, 237–248.

Cohen, S.L., Ferre-D'Amare, A.R., Burley, S.K., and Chait, B.T. (1995b). Probing the solution structure of the DNA-binding protein Max by a combination of proteolysis and mass spectrometry. Protein Sci. *4*, 1088–1099.

Daniel, M.D., Kirchoff, F., Czajak, S.C., Sehgal, P.K., and Derosiers, R.C. (1992). Protective effects of a live attenuated SIV vaccine with a deletion in the nef gene. Science *258*, 1938–1941.

Deacon, N.J., Tsykin, A., Solomon, A., Smith, K., Ludford-Menting, M., Hooker, D.J., McPhee, D.A., Greenway, A.L., Ellett, A., Chatfield, C., Lawson, V.A., Crowe, S., Maerz, A., Sonza, S., Learmont, J., Sullivan, J.S., Cunningham, A., Dwyer, D., Dowton, D., and Mills, J. (1995). Genomic structure of an attenuated quasi species of HIV-1 from a blood transfusion donor and recipients. Science *270*, 988–991.

Feng, S., Chen, J.K., Yu, H., Simon, J.A., and Schreiber, S.A. (1994). Two binding orientations for peptides to the Src SH3 domain: development of a general model for SH3-ligand interactions. Science *266*, 1241–1247.

Feng, S., Kasahara, C., Rickles, R.J., and Schreiber, S.L. (1995). Specific interactions outside the proline-rich core of two classes of Src homology 3 ligands. Proc. Natl. Acad. Sci. USA *92*, 12408–12415.

Freund, J., Kellner, R., Houthaeve, T., and Kalbitzer, H.R. (1994a). Stability and proteolytic domains of Nef protein from human immunodeficiency virus (HIV) type 1. Eur. J. Biochem. *221*, 811–819.

Freund, J., Kellner, R., Konvalinka, J., Wolber, V., Kräusslich, H.-G., and Kalbitzer, H.R. (1994b). A possible regulation of negative factor (Nef) activity of human immunodeficiency virus type 1 by the viral protease. FEBS Lett. *223*, 589–593.

Gosser, Y.Q., Zheng, J., Overduin, M., Mayer, B.J., and Cowburn, D. (1995). The solution structure of Abl SH3, and its relationship to SH2 in the SH(32) construct. Structure *3*, 1075–1086.

Goudreau, N., Cornille, F., Duchesne, M., Parker, F., Tocqué, B., Garbay, C., and Roques, B.P. (1994). NMR structure of the N-terminal SH3 domain of GRB2 and its complex with a proline rich peptide from Sos. Nature Struct. Biol. *1*, 898–907.

Grzesiek, S., Wingfield, P., Stahl, S., Kaufman, J.D., and Bax, A. (1995). Four-dimensional 15N-separated NOESY of slowly tumbling perdeuterated 15N-enriched proteins: applications to HIV-1 Nef. J. Am. Chem. Soc. *117*, 9594–9595.

Grzesiek, S., Bax, A., Clore, G.M., Gronenborn, A.M., Hu, J.-S., Kaufman, J., Palmer, I., Stahl, S.J., and Wingfield, P.T. (1996). The solution structure of HIV-1 Nef reveals an unexpected fold and permits delineation of the binding surface for the SH3 domain of Hck tyrosine protein kinase. Nature Struct. Biol. *3*, 340–345.

Hendrickson, W.A. (1991). Determination of macromolecular structures from anomalous diffraction of synchrotron data. Science *254*, 51–58.

Huang, Y., Zhang, L., and Ho, D.D. (1995). Characterization of nef sequences in long-term survivors of human immunodeficiency virus type 1 infection. J. Virol. *69*, 93–100.

Jones, T.A., Zou, J.Y., Cowan, S. W., and Kjeldgaard, M. (1991). Improved methods for building protein models in electron density maps and the location of errors in these models. Acta Cryst. *A47*, 110–119.

Kestler, H.W., III, Ringler, D.J., Mori, K., Panicali, D.L., Sehgal, P.K., Daniel, M.D., and Desrosiers, R.C. (1991). Importance of the *nef* gene for maintenance of high virus loads and for development of AIDS. Cell *65*, 651–662.

Kirchhoff, F., Greenough, T.C., Brettler, D.B., Sullivan, J.L., and Desrosiers, R.C. (1995). Absence of intact nef sequences in a long-term survivor with nonprogressive HIV-1 infection. N. Engl. J. Med. *332*, 259–260.

Knudsen, B., Zheng, J., Feller, S.M., Mayer, J.P., Burrell, S.K., Cowburn, D., and Hanafusa, H. (1995). Affinity and specificity requirements for the first Src homology 3 domain of the Crk protein. EMBO J. *14*, 2191–2198.

Kraulis, P. (1991). MOLSCRIPT: a program to produce both detailed and schematic plots of protein structures. J. Appl. Cryst. *24*, 946–950.

Lee, C.-H., Leung, B., Lemmon, M.A., Zheng, J., Cowburn, D., Kuriyan, J., and Saksela, K. (1995). A single amino acid in the SH3 domain of Hck determines its high affinity and specificity in binding to HIV-1 Nef protein. EMBO J. *14*, 5006–5015.

Lim, W.A., and Richards, F.M. (1994). Critical residues in an SH3 domain from Sem-5 suggest a mechanism for proline-rich peptide recognition. Nature Struct. Biol. *1*, 221–225.

Lim, W.A., Richards, F.M., and Fox, R.O. (1994). Structural determinants of peptide-binding orientation and of sequence specificity in SH3 domains. Nature *372*, 375–379.

Nicholls, A., Sharp, K.A., and Honig, B. (1991). Protein folding and association: insights from the interfacial and thermodynamic properties of hydrocarbons. Proteins *11*, 281–296.

Noble, M.E.M., Musacchio, A., Saraste, M., Courtneidge, S.A., and Wierenga, R.K. (1993). Crystal structure of the SH3 domain in human Fyn: comparison of the three-dimensional structures of SH3 domains in tyrosine kinases and spectrin. EMBO J. *12*, 2617–2624.

Pawson, T. (1995). Protein modules and signalling networks. Nature *373*, 573–580.

Ren, R., Mayer, B.J., Cicchetti, P., and Baltimore, D. (1993). Identification of a ten-amino acid proline-rich SH3 binding site. Science *259*, 1157–1161.

Saksela, K., Cheng, G., and Baltimore, D. (1995). Proline-rich (PxxP) motifs in HIV-1 Nef bind to SH3 domains of a subset of Src kinases and are required for the enhanced growth of Nef+ viruses but not for down-regulation of CD4. EMBO J. *14*, 484–491.

Sawai, E.T., Baur, A., Struble, H., Peterlin, B.M., Levy, J. A., and Cheng-Mayer, C. (1994). Human immunodeficiency virus type I Nef associates with a cellular serine kinase in T lymphocytes. Proc. Natl. Acad. Sci. USA *91*, 1539–1543.

Sawai, E.T., Baur, A.S., Peterlin, B.M., Levy, J.A., and Cheng-Mayer, C. (1995). A conserved domain and membrane targeting of Nef from HIV and SIV are required for association with a cellular serine kinase activity. J. Biol. Chem. *270*, 15307–15314.

Shugars, D.C., Smith, M.S., Glueck, D.H., Nantermet, P.V., Seillier-Moiseiwitsch, F., and Swanstrom, R. (1993). Analysis of human immunodeficiency virus type 1 nef gene sequences present *in vivo.* J. Virol. *67*, 4639–4650.

Terasawa, H., Kohda, D., Hatanaka, H., Tsuchiya, S., Ogura, K., Nagata, K., Ishii, S., Mandiyan, V., Ullrich, A., Schlessinger, J., and Inagaki, F. (1994). Structure of the N-terminal SH3 domain of GRB2 complexed with a peptide from the guanine nucleotide releasing factor Sos. Nature Struct. Biol. *1*, 891–897.

Trono, D. (1995). HIV accessory proteins: leading roles for the supporting cast. Cell *82*, 189–192.

Weis, W.I., Kahn, R., Fourme, R., Drickamer, K., and Hendrickson, W.A. (1991). Structure of the calcium-dependent lectin domain from a rat mannose-binding protein determined by MAD phasing. Science *254*, 1608–1615.

Wu, X., Knudsen, B., Feller, S.M., Zheng, J., Sali, A., Cowburn, D., Hanafusa, H., and Kuriyan, J. (1995). Structural basis for the specific interaction of lysine-containing proline-rich peptides with the N-terminal SH3 domain of c-Crk. Structure *3*, 215–226.

Yu, H., Chen, J.K., Feng, S., Dalgarno, D.C., Brauer, A.W., and Schreiber, S.L. (1994). Structural basis for the binding of proline-rich peptides to SH3 domains. Cell *76*, 933–945.

Zhang, K.Y.J., and Main, P. (1990). The use of Sayre's equation with solvent flattening and histogram matching for phase extension and refinement of protein structures. Acta Cryst. *A46*, 377–381.